Noname manuscript No.
(will be inserted by the editor)

Discontinuity-induced bifurcations of a dual-point contact ball

Mate Antali · Gabor Stepan

Last version: 2016.12.07.

Abstract In this paper, dynamics of a ball is investigated, which is in dual-point contact with a cylindrical vessel. This model is based on a concept of a type of flowmeter. Rolling, slipping and separation of surfaces can all occur at both contact points, which results in a nonsmooth dynamical system. Stationary solutions of the system and their stability are determined in the different kinematic cases. By introducing the concept of stability with respect to slipping, existence of the stationary solutions can be checked even in the case when the contact forces are undetermined. Discontinuity-induced bifurcations of the system are explored.

Keywords dual-point contact, flowmeter, nonsmooth dynamics, discontinuity-induced bifurcations

Introduction

One of the basic principles of flow rate measurement is to place a solid body into the fluid and to let it be moved or rotated by the fluid flow. One possible concept of this idea can be seen in Fig. 1, which can be found in several accepted patents from the last decades. A metal ball is placed into an axisymmetric vessel, in which swirling flow is created by blades or other geometric solutions at the inlet. The swirling flow makes the ball roll round along the edge of the vessel. The velocity of the ball can be measured e.g. by an inductive sensor outside the vessel. After calibration, the flow rate of the fluid can be determined. This concept is called *cyclonic flowmeter* [9] or *orbital ball flowmeter* [27] in the literature.

For the application of this concept, one of the earliest patents was submitted by Kearsley [17] already in 1950. Since then, several similar patents were applied [11,30,7, 9], and new variations for the geometry were introduced [15, 33]) even in the recent years [26,27]. Contrary to the large number of the patents, dynamics of the ball has not been investigated analytically.

Dynamics of the ball in the flowmeter is based on the dual-point contact kinematics, which means that the two bodies involved have two contact points during the motion. This problem can be found in other fields of mechanical engineering. For example, kinematic oscillation of railway wheelsets has the same kinematic scenario [32,25], which was recently analysed by the authors [2,1]. Similar kinematics can be found in roller bearings. In tapered roller bearings [34] and in angular contact ball bearings [3,24,14], rolling elements have essentially the same constraints as the ball in the flowmeter.

In this paper, dynamics of the ball is investigated analytically in the case of stationary flow of the fluid. Even for this simple excitation from the flow, behaviour of the ball becomes complicated due to the several kinematic cases related to slipping and unilateral contact at the contact points. As we focus on *qualitative* description of the system, the flow field in the vessel and its effect on the ball is simplified as much as possible.

In Section 1, the mechanical model is created and the equations of motion are derived for all kinematic cases of the system. After determining the stationary solutions of the ball, we identify the parameter values for which the stationary solutions exist (Section 2). However, it cannot be done in the case of dual-point rolling due to the undetermined con-

Mate Antali
Department of Applied Mechanics, Budapest University of Technology and Economics, Budapest, H-1521, Hungary
E-mail: antali@mm.bme.hu

Gabor Stepan
Department of Applied Mechanics, Budapest University of Technology and Economics, Budapest, H-1521, Hungary
E-mail: stepan@mm.bme.hu

Gabor Stepan
HAS-BME Research Group on Dynamics of Machines and Vehicles, Hungarian Academy of Sciences, Budapest H-1521, Hungary

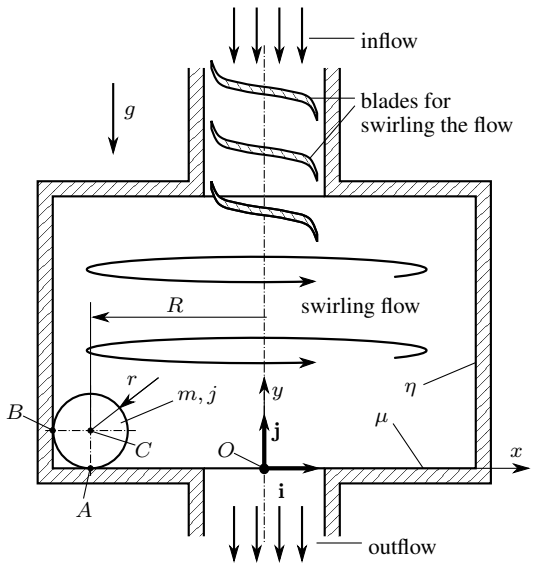

Fig. 1 Sketch of the mechanical model. The swirling flow of the fluid makes the ball travel round along the edge of the vessel.

Notation	Quantity	Dimen.
m	mass of the ball	kg
r	radius of the ball	m
j	dimensionless moment of inertia of the ball	–
$R+r$	radius of the vessel	m
μ	friction coefficient between the ball and the bottom of the vessel	–
η	friction coefficient between the ball and the wall of the vessel	–
g	reduced gravitational acceleration (including buoyancy)	$\mathrm{m/s^2}$
ω_0	stationary angular velocity of the fluid	$1/\mathrm{s}$
$m \cdot c$	viscous drag coefficient	$\mathrm{kg \cdot m/s}$

Table 1 List of physical parameters.

tact forces. This problem can be solved by a new method introduced in Section 3, which is applied in the case of dual-point rolling in Section 4. Based on these results, the bifurcations of the system are characterised (Section 5) and limitations of this type of flowmeters are identified.

1 Mechanical model

Let us consider a cylindrical vessel that guides the ball. This is one of the simplest possible geometries (see Fig. 1), which can be found in [9]. Let the ball have a radius of r, and let the inner radius of the cylinder be equal to $R+r$ (see Table 1 for the list of the parameters).

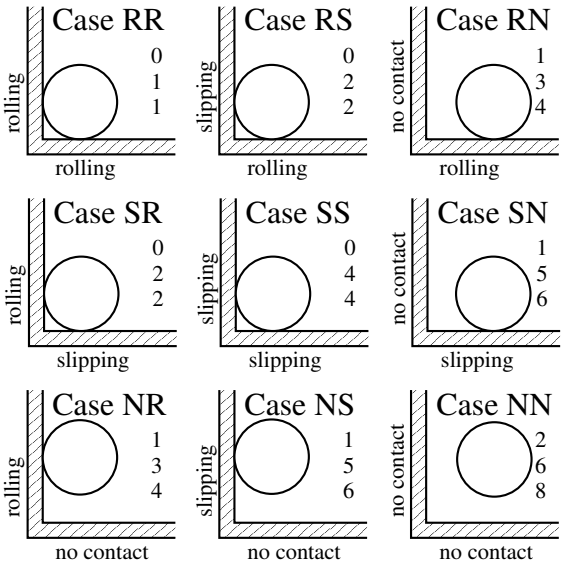

Fig. 2 Kinematic cases of the ball. The two characters of the acronym describe the type of contact with the bottom and the wall, respectively. Rolling, slipping and no contact are denoted by capital letters R, S and N, respectively. In each panel, the three numbers are: the number of necessary variables to describe the geometric state, the number of independent quasi-velocities and the dimension of state space, respectively.

1.1 Kinematic cases

Let A denote the downmost point of the ball, where contact can occur with the bottom of the vessel . Similarly, let B denote the outermost point of the ball, which can be in contact with the wall of the vessel. At a contact point between the bodies, three possible situations can occur. The ball can be in rolling or slipping contact with the vessel, or the ball can be separated from the surface of the vessel. For the contact points A and B, this results in 9 different kinematic cases (see Fig. 2). Throughout the paper, different kinematic cases are denoted by two-letter acronyms, the first letter corresponds to point A, the second refers to point B. Both letters of the acronyms can be R (rolling contact), S (slipping contact) or N (no contact), depending on the state of the contact (see Fig. 2).

In this paper, we focus on the stationary solutions of the ball. It is physically foreseeable that in cases with no contact with the wall (Cases RN, SN and NN), no such stationary motion is realisable. Therefore, the analysis is restricted to the 6 cases of the first two columns of Fig. 2.

1.2 Kinematics

The components of the vectors are computed in a coordinate system co-rotating with the *centre* of the ball. The basis vectors of this Cartesian coordinate system are denoted by **i**, **j**, **k**, where **i** points radially inwards, **j** points axially upwards

Notation	Phase variable	Dimen.
y	axial displacement	m
v_y	axial velocity	m/s
ω_c	angular velocity of the coordinate system co-rotating with the centre of the ball	1/s
$\tilde{\omega}_x$	radial angular velocity of slipping	1/s
$\tilde{\omega}_y$	axial angular velocity of slipping	1/s
$\tilde{\omega}_z$	tangential angular velocity of slipping	1/s
Notation	**Auxiliary variable**	**Dimen.**
v_A	slipping velocity at point A	m/s
v_B	slipping velocity at point B	m/s
α	slipping direction at point A	–
β	slipping direction at point B	–

Table 2 List of variables. Phase variables are used to describe the state of the system uniquely (see also (19) and Table 4). Auxiliary variables are used in some parts of the paper to simplify calculations.

and $\mathbf{k}$ is defined by $\mathbf{k} := \mathbf{i} \times \mathbf{j}$, where $\times$ denotes the cross product of vectors. Let the origin O of the coordinate system be located in the middle of the bottom of the vessel. In this coordinate system, the location of the centre C of the ball is given by

$$\mathbf{r}_{OC} = \begin{bmatrix} -R \\ r+y \\ 0 \end{bmatrix}, \tag{1}$$

where $y(t)$ is the axial displacement of the ball. At $y = 0$, the ball touches the bottom of the vessel. The notation of all phase variables can be found in Table 2. Throughout the paper, dependence of variables on the time t is indicated only if it is necessary.

Let us denote the angular velocity of the co-rotating coordinate system by $\boldsymbol{\omega}_c(t) = \omega_c(t)\mathbf{j}$. Then, by calculating the time derivatives in this rotating coordinate system, the velocity and acceleration of the centre of the ball are given by

$$\mathbf{v}_C = \dot{\mathbf{r}}_{OC} + \boldsymbol{\omega}_c \times \mathbf{r}_{OC} = \begin{bmatrix} 0 \\ v_y \\ R\omega_c \end{bmatrix} \tag{2}$$

and

$$\mathbf{a}_C = \dot{\mathbf{v}}_C + \boldsymbol{\omega}_c \times \mathbf{v}_C = \begin{bmatrix} R\omega_c^2 \\ \dot{v}_y \\ R\dot{\omega}_c \end{bmatrix}, \tag{3}$$

respectively, where $v_y(t) := \dot{y}(t)$ is the axial velocity of the ball.

The angular velocity $\boldsymbol{\omega}$ of the ball can be split up into a *rolling* part $\bar{\boldsymbol{\omega}}$ and a *slipping* part $\tilde{\boldsymbol{\omega}}$ in the form

$$\boldsymbol{\omega} = \bar{\boldsymbol{\omega}} + \tilde{\boldsymbol{\omega}} = \begin{bmatrix} \frac{R}{r}\omega_c \\ -\frac{R}{r}\omega_c \\ \frac{1}{r}v_y \end{bmatrix} + \begin{bmatrix} \tilde{\omega}_x \\ \tilde{\omega}_y \\ \tilde{\omega}_z \end{bmatrix}, \tag{4}$$

where $\tilde{\omega}_x(t)$, $\tilde{\omega}_y(t)$ and $\tilde{\omega}_z(t)$ are the slipping components of the angular velocity. By differentiating (4) as we did in (3), we obtain that the angular acceleration $\boldsymbol{\varepsilon}$ of the ball is

$$\boldsymbol{\varepsilon} = \begin{bmatrix} \frac{R}{r}\dot{\omega}_c + \frac{1}{r}\omega_c v_y + \dot{\tilde{\omega}}_x + \omega_c\tilde{\omega}_z \\ -\frac{R}{r}\dot{\omega}_c + \dot{\tilde{\omega}}_y \\ \frac{1}{r}\dot{v}_y - \frac{R}{r}\omega_c^2 + \dot{\tilde{\omega}}_z - \omega_c\tilde{\omega}_x \end{bmatrix}. \tag{5}$$

The possible contact points A and B are located at $\mathbf{r}_{CA} = -r\mathbf{j}$ and $\mathbf{r}_{CB} = -r\mathbf{i}$. Their velocities are given by

$$\mathbf{v}_A = \begin{bmatrix} r\tilde{\omega}_z \\ 0 \\ -r\tilde{\omega}_x \end{bmatrix}, \qquad \mathbf{v}_B = \begin{bmatrix} 0 \\ -r\tilde{\omega}_z \\ r\tilde{\omega}_y \end{bmatrix}, \tag{6}$$

thus, the kinematic conditions of rolling at A or B are satisfied exactly when the corresponding slipping angular velocities are zero. In order to simplify some subsequent calculations, let us express (6) in polar coordinates by defining the *slipping velocities*

$$v_A := r\sqrt{\tilde{\omega}_z^2 + \tilde{\omega}_x^2}, \qquad v_B := r\sqrt{\tilde{\omega}_z^2 + \tilde{\omega}_y^2} \tag{7}$$

and the *slipping directions*

$$\alpha := \arctan(\tilde{\omega}_x, \tilde{\omega}_z), \qquad \beta := \arctan(\tilde{\omega}_y, \tilde{\omega}_z). \tag{8}$$

1.3 Forces

The gravity field points axially downwards and results in the force $\mathbf{F}_g = -mg\mathbf{j}$, where g is the *reduced* gravitational acceleration including the buoyancy effect of the fluid. The effect of the fluid flow is simplified as much as possible to focus on the essence of the problem. We assume that in the outer region of the vessel the fluid has a rigid-body-like motion and it rotates with a constant angular velocity $\boldsymbol{\omega}_0 = \omega_0\mathbf{j}$. The velocity of the fluid at point C is calculated as $\mathbf{v}_{fC} = \boldsymbol{\omega}_0 \times \mathbf{r}_{OC} = \omega_0 R\mathbf{k}$. The viscous force $\mathbf{F}_f$ is modelled by Stokes' drag law (see e.g. [28], p. 451.),

$$\mathbf{F}_f = -mc\,(\mathbf{v}_C - \mathbf{v}_{fC}) = \begin{bmatrix} 0 \\ -mcv_y \\ -mcR(\omega_c - \omega_0) \end{bmatrix}. \tag{9}$$

The drag coefficient is written in the form mc to make the calculations easier, and c can be calculated as

$$c = \frac{9\nu_f}{2r^2} \cdot \frac{\rho_f}{\rho_b}. \tag{10}$$

Here, ν_f is the kinematic viscosity of the fluid, and ρ_b, ρ_f denote the density of the ball and the fluid, respectively. We do not make effort to model the effect of the fluid accurately (as it is done e.g. in [29] and [18]) because the approximate value of the linear coefficient c is sufficient for qualitative analysis. If we assume water and a steel ball with a diameter

of a few millimetres then the order of magnitude of the value of c is $10^{-2}\,1/\mathrm{s}$, and it is much smaller in the case of gases.

For modelling the contact at one of the contact points, we assume single-point contact because the loading forces are very small compared to the stiffness of the parts. Hence, we consider the concentrated contact forces

$$\mathbf{F}_A = \begin{bmatrix} A_x \\ A_y \\ A_z \end{bmatrix}, \qquad \mathbf{F}_B = \begin{bmatrix} B_x \\ B_y \\ B_z \end{bmatrix}. \tag{11}$$

In the case of no contact, the contact force vanishes ($\mathbf{F}_A = \mathbf{0}$ or $\mathbf{F}_B = \mathbf{0}$). In the case of rolling and slipping, we require non-negative normal force at the corresponding contact point, that is,

$$A_y \geq 0, \qquad B_x \geq 0. \tag{12}$$

In the case of rolling, we assume that the tangential forces are restricted by the simple Coulomb model,

$$\sqrt{A_x^2 + A_z^2} \leq \mu A_y, \qquad \sqrt{B_y^2 + B_z^2} \leq \eta B_x, \tag{13}$$

where μ and η are the friction coefficients on the bottom and on the wall, respectively.

In the case of slipping, the formulae

$$\mathbf{F}_A = A_y(\mathbf{j} - \mu\,\mathbf{dir}\,\mathbf{v}_A), \qquad \tilde{\omega}_x^2 + \tilde{\omega}_z^2 \neq 0, \tag{14}$$

$$\mathbf{F}_B = B_x(\mathbf{i} - \eta\,\mathbf{dir}\,\mathbf{v}_B), \qquad \tilde{\omega}_y^2 + \tilde{\omega}_z^2 \neq 0 \tag{15}$$

can be used if we assume the same friction coefficients for static and dynamic friction. For a non-zero vector $\mathbf{v}$, the direction function $\mathbf{dir}\,\mathbf{v} := \mathbf{v}/\|\mathbf{v}\|$ assigns the corresponding unit vector, thus, (14) is equivalent to

$$A_x = -\mu A_y \frac{\tilde{\omega}_z}{\sqrt{\tilde{\omega}_z^2+\tilde{\omega}_x^2}}, \qquad A_z = \mu A_y \frac{\tilde{\omega}_x}{\sqrt{\tilde{\omega}_z^2+\tilde{\omega}_x^2}}, \tag{16}$$

and (15) leads to

$$B_y = \eta B_x \frac{\tilde{\omega}_z}{\sqrt{\tilde{\omega}_z^2+\tilde{\omega}_y^2}}, \qquad B_z = -\eta B_x \frac{\tilde{\omega}_y}{\sqrt{\tilde{\omega}_z^2+\tilde{\omega}_y^2}}. \tag{17}$$

To obtain a better approximation for the contact in water, a velocity-dependent friction coefficient $\bar{\mu}(\|\mathbf{v}_A\|)$ could also be used instead of μ. Then, (14) could be replaced by

$$\mathbf{F}_A = A_y\left(\mathbf{j} - \bar{\mu}(\|\mathbf{v}_A\|) \cdot \mathbf{dir}\,\mathbf{v}_A\right), \tag{18}$$

where $\bar{\mu}(0) = \mu$, and this generalisation could also be done for $\mathbf{F}_B$ and η. In this paper, we restrict our calculations to the simple Coulomb model (13)-(15), which proves to be effective for qualitative analysis. Even for the more realistic Stribeck model, there exists a low velocity range called *boundary lubrication* where the static friction coefficient is a good approximation of the characteristic curve (see e.g. [22], p. 761). Thus, the simple Coulomb model is satisfactory to grab the essence of our problem here. We neglect the effect of the difference between static and dynamic friction coefficients (see e.g. [31]) and the effect of drilling friction (see e.g. [23]).

Case	Constraints	Known forces
RR	$\tilde{\omega}_x = \tilde{\omega}_y = \tilde{\omega}_z \equiv 0$, $v_y \equiv 0, \quad (y \equiv 0)$	
RS	$\tilde{\omega}_x = \tilde{\omega}_z \equiv 0$, $v_y \equiv 0, \quad (y \equiv 0)$	$\mathbf{F}_B = B_x(\mathbf{i} - \eta\,\mathbf{dir}\,\mathbf{v}_B)$
SR	$\tilde{\omega}_y = \tilde{\omega}_z \equiv 0$, $v_y \equiv 0, \quad (y \equiv 0)$	$\mathbf{F}_A = A_y(\mathbf{j} - \mu\,\mathbf{dir}\,\mathbf{v}_A)$
SS	$v_y \equiv 0, \quad (y \equiv 0)$	$\mathbf{F}_B = B_x(\mathbf{i} - \eta\,\mathbf{dir}\,\mathbf{v}_B)$ $\mathbf{F}_A = A_y(\mathbf{j} - \mu\,\mathbf{dir}\,\mathbf{v}_A)$
NR	$\tilde{\omega}_y = \tilde{\omega}_z \equiv 0$, $y \geq 0$	$\mathbf{F}_A = 0$
NS	$y \geq 0$	$\mathbf{F}_A = 0$ $\mathbf{F}_B = B_x(\mathbf{i} - \eta\,\mathbf{dir}\,\mathbf{v}_B)$

Table 3 Constraints and known forces for the different kinematic cases.

1.4 Equations of motion of the kinematic cases

As we can see from (2) and (4), the state of velocity of the ball can be described by the variables $v_y, \omega_c, \tilde{\omega}_x, \tilde{\omega}_y$ and $\tilde{\omega}_z$. These five quantities can be called *quasi-velocities* (see e.g. [13], p. 217). After considering the spherical symmetry of the ball (3-dimensional) and the cylindrical symmetry of the vessel (1-dimensional), the geometric state of the ball can be described by the single variable $y \geq 0$. Therefore, the state of the system can be given by the vector

$$\mathbf{x} = \begin{bmatrix} y & v_y & \omega_c & \tilde{\omega}_x & \tilde{\omega}_y & \tilde{\omega}_z \end{bmatrix}^T \in X \tag{19}$$

of the state space $X \cong \mathbb{R}^6$.

The mass moment of inertia matrix is denoted by $\mathbf{J} = jmr^2\mathbf{I}$, where j is the dimensionless moment of inertia and $\mathbf{I}$ is the identity matrix. The value of j is between 0 and $2/3$. In the case of uniform mass distribution, $j = 2/5$. By using the results of the previous subsections, Newton's Second Law for rigid bodies can be written in the form

$$\begin{cases} \mathbf{F}_g + \mathbf{F}_A + \mathbf{F}_B + \mathbf{F}_f & = m\mathbf{a}_C, \\ \mathbf{r}_{CA} \times \mathbf{F}_A + \mathbf{r}_{CB} \times \mathbf{F}_B & = \mathbf{J}\boldsymbol{\varepsilon} + \boldsymbol{\omega} \times \mathbf{J}\boldsymbol{\omega}. \end{cases} \tag{20}$$

Together with the relation between y and v_y, equation (20) leads to a set of differential-algebraic equations (DAEs),

$$\begin{cases} A_x + B_x = m\omega_c^2 R, \\ A_y + B_y - m(g + cv_y) = m\dot{v}_y, \\ A_z + B_z - mRc(\omega_c - \omega_0) = mR\dot{\omega}_c, \\ -A_z r = jmr^2\left(\frac{R}{r}\dot{\omega}_c + \frac{1}{r}\omega_c v_y + \dot{\tilde{\omega}}_x + \omega_c\tilde{\omega}_z\right), \\ B_z r = jmr^2\left(-\frac{R}{r}\dot{\omega}_c + \dot{\tilde{\omega}}_y\right), \\ A_x r - B_y r = jmr^2\left(\frac{1}{r}\dot{v}_y - \frac{R}{r}\omega_c^2 + \dot{\tilde{\omega}}_z - \omega_c\tilde{\omega}_x\right), \\ \dot{y} = v_y. \end{cases} \tag{21}$$

For a full set of DAEs in $\mathbf{x}$, $\mathbf{F}_A$ and $\mathbf{F}_B$, (21) has to be extended by 5 additional scalar equations.

For the different kinematic cases, these missing equations can be obtained from the constraints and from the known

contact force components, which can be seen in Table 3. For all cases but Case RR, we have the additional 5 independent scalar equations, which lead to a linear system of DAEs with a unique solution. In Case RR, there are only 4 equations, which leads to indeterminacy in the contact forces. By using (21) and Table 3, a system of first-order ordinary differential equations (ODEs) can be created in the form

$$\dot{\mathbf{x}} = \mathbf{f}_{\mathrm{RR}}(\mathbf{x}), \qquad \dots \qquad \dot{\mathbf{x}} = \mathbf{f}_{\mathrm{NS}}(\mathbf{x}), \tag{22}$$

for all the six cases (see Table 4 for the notations). The formulae of the vector fields for the different cases are

$$\mathbf{f}_{\mathrm{RR}}(\mathbf{x}) = \begin{bmatrix} 0 \\ 0 \\ -\frac{c(\omega_c-\omega_0)}{1+2j} \\ 0 \\ 0 \\ 0 \end{bmatrix}, \tag{23}$$

$$\mathbf{f}_{\mathrm{RS}}(\mathbf{x}) = \begin{bmatrix} 0 \\ 0 \\ -\frac{c(\omega_c-\omega_0)}{1+j}+\frac{B_z^{\mathrm{RS}}}{(1+j)mR} \\ 0 \\ -\frac{cR(\omega_c-\omega_0)}{(1+j)r}+\frac{(1+2j)B_z^{\mathrm{RS}}}{j(1+j)mr} \\ 0 \end{bmatrix}, \tag{24}$$

$$\mathbf{f}_{\mathrm{SR}}(\mathbf{x}) = \begin{bmatrix} 0 \\ 0 \\ -\frac{c(\omega_c-\omega_0)}{1+j}+\frac{A_z^{\mathrm{SR}}}{(1+j)mR} \\ \frac{cR(\omega_c-\omega_0)}{(1+j)r}-\frac{(1+2j)A_z^{\mathrm{SR}}}{j(1+j)mr} \\ 0 \\ 0 \end{bmatrix}, \tag{25}$$

$$\mathbf{f}_{\mathrm{SS}}(\mathbf{x}) = \begin{bmatrix} 0 \\ 0 \\ -c(\omega_c-\omega_0)+\frac{A_z^{\mathrm{SS}}+B_z^{\mathrm{SS}}}{mR} \\ \frac{cR(\omega_c-\omega_0)}{r}-\omega_c\tilde{\omega}_z-\frac{(1+j)A_z^{\mathrm{SS}}+jB_z^{\mathrm{SS}}}{jmr} \\ \frac{-cR(\omega_c-\omega_0)}{r}+\frac{jA_z^{\mathrm{SS}}+(1+j)B_z^{\mathrm{SS}}}{jmr} \\ \frac{R}{r}\omega_c^2+\omega_c\tilde{\omega}_x+\frac{\tilde{\omega}_z A_z^{\mathrm{SS}}}{\tilde{\omega}_x jmr}+\frac{\tilde{\omega}_z B_z^{\mathrm{SS}}}{\tilde{\omega}_y jmr} \end{bmatrix}, \tag{26}$$

$$\mathbf{f}_{\mathrm{NR}}(\mathbf{x}) = \begin{bmatrix} v_y \\ \frac{-cv_y-g+jr\left(\tilde{\omega}_x\omega_c+\frac{R}{r}\omega_c^2\right)}{1+j} \\ -\frac{c(\omega_c-\omega_0)}{1+j} \\ \frac{cR(\omega_c-\omega_0)}{(1+j)r}-\frac{\omega_c v_y}{r} \\ 0 \\ 0 \end{bmatrix}, \tag{27}$$

Case	Domain	Active variables	Dynamics
RR	$X_{\mathrm{RR}} \cong \mathbb{R}^1$	ω_c	$\mathbf{f}_{\mathrm{RR}}$
RS	$X_{\mathrm{RS}} \cong \mathbb{R}^2$	$\omega_c, \tilde{\omega}_x$	$\mathbf{f}_{\mathrm{RS}}$
SR	$X_{\mathrm{SR}} \cong \mathbb{R}^2$	$\omega_c, \tilde{\omega}_y$	$\mathbf{f}_{\mathrm{SR}}$
SS	$X_{\mathrm{SS}} \cong \mathbb{R}^4$	$\omega_c, \tilde{\omega}_x, \tilde{\omega}_y, \tilde{\omega}_z$	$\mathbf{f}_{\mathrm{SS}}$
NR	$X_{\mathrm{NR}} \cong \mathbb{R}^4$	$y, v_y, \omega_c, \tilde{\omega}_y$	$\mathbf{f}_{\mathrm{NR}}$
NS	$X_{\mathrm{NS}} \cong \mathbb{R}^6$	$y, v_y, \omega_c, \tilde{\omega}_x, \tilde{\omega}_y, \tilde{\omega}_z$	$\mathbf{f}_{\mathrm{NS}}$

Table 4 Notations for the dynamics of the different kinematic cases. The domains of the different cases are subspaces of the whole space $X = X_{\mathrm{NS}}$, they are defined by the constraints (see the second column of Table 3).

$$\mathbf{f}_{\mathrm{NS}}(\mathbf{x}) = \begin{bmatrix} v_y \\ -cv_y-g-\frac{\tilde{\omega}_z B_z^{\mathrm{NS}}}{\tilde{\omega}_x m} \\ -c(\omega_c-\omega_0)+\frac{B_z^{\mathrm{NS}}}{mR} \\ \frac{cR(\omega_c-\omega_0)}{r}-\omega_c\tilde{\omega}_z-\frac{\omega_c v_y}{r}-\frac{B_z^{\mathrm{NS}}}{mr} \\ \frac{-cR(\omega_c-\omega_0)}{r}+\frac{(1+j)B_z^{\mathrm{NS}}}{jmr} \\ \frac{R}{r}\omega_c^2+\omega_c\tilde{\omega}_x-\frac{cv_y+g}{r}+\frac{\tilde{\omega}_z(1+j)B_z^{\mathrm{NS}}}{\tilde{\omega}_x jmr} \end{bmatrix}, \tag{28}$$

where the expressions of the corresponding contact force components are

$$\begin{aligned}
B_z^{\mathrm{RS}} &:= -\eta(1+j)mR\omega_c^2 \operatorname{sgn}\tilde{\omega}_y, \\
A_z^{\mathrm{SR}} &:= \mu m\left(g - jR\omega_c^2 - jr\omega_c\tilde{\omega}_x\right)\operatorname{sgn}\tilde{\omega}_x, \\
A_z^{\mathrm{SS}} &:= \frac{mg - m\omega_c^2 R\eta\frac{\tilde{\omega}_z}{\sqrt{\tilde{\omega}_z^2+\tilde{\omega}_y^2}}}{1+\eta\mu\frac{\tilde{\omega}_z}{\sqrt{\tilde{\omega}_z^2+\tilde{\omega}_x^2}}\frac{\tilde{\omega}_z}{\sqrt{\tilde{\omega}_z^2+\tilde{\omega}_y^2}}}\cdot\mu\frac{\tilde{\omega}_x}{\sqrt{\tilde{\omega}_z^2+\tilde{\omega}_x^2}}, \\
B_z^{\mathrm{SS}} &:= \frac{-m\omega_c^2 R - mg\mu\frac{\tilde{\omega}_z}{\sqrt{\tilde{\omega}_z^2+\tilde{\omega}_x^2}}}{1+\eta\mu\frac{\tilde{\omega}_z}{\sqrt{\tilde{\omega}_z^2+\tilde{\omega}_x^2}}\frac{\tilde{\omega}_z}{\sqrt{\tilde{\omega}_z^2+\tilde{\omega}_y^2}}}\cdot\eta\frac{\tilde{\omega}_y}{\sqrt{\tilde{\omega}_z^2+\tilde{\omega}_y^2}}, \\
B_z^{\mathrm{NS}} &:= -\eta mR\omega_c^2\frac{\tilde{\omega}_y}{\sqrt{\tilde{\omega}_z^2+\tilde{\omega}_y^2}}.
\end{aligned} \tag{29}$$

The set of vector fields (23)-(28) determines the dynamics for all kinematic cases. By considering the active (unconstrained) variables, we have a rough picture of the 6-dimensional state space X. In Fig. 3, the sketch of some typical sections of the state space can be seen with the corresponding kinematic cases. In Table 4, notations for the different cases are presented.

2 Stationary solutions

We investigate the stationary solutions of (22), which belong to *stationary motions* of the mechanical system. During these stationary motions, the centre of the ball travels round the vessel with a constant velocity, and its angular velocity is also constant in the rotating coordinate system. Operation of the flowmeter is based on these stationary motions: for a constant flow velocity (characterised by ω_0), the centre of the ball should have a constant velocity along the circumference of the vessel (characterised by $\omega_c(t) \equiv \omega_c^0$).

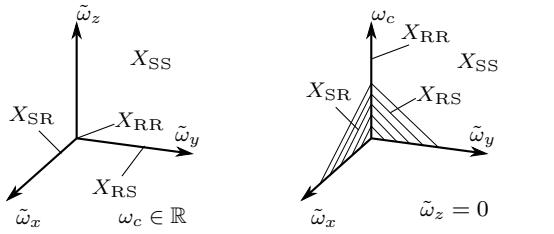

Fig. 3 Sections of the state space X. Left panel: section of $y = 0$, $v_y = 0$, $\omega_c \in \mathbb{R}$, right panel: section of $y = 0$, $v_y = 0$, $\tilde{\omega}_z = 0$. Cases RS and SR are located on planes which intersect each other in a line containing Case RR. Therefore, Cases SR and RS lay in the same 3-dimensional section (left panel) of the 4-dimensional space of X_{SS}. Case SR is also embedded into a 4-dimensional space of X_{NR}, and Case NS fills the 6-dimensional state space $X = X_{\mathrm{NS}}$.

To obtain the stationary solutions, let us substitute $\mathbf{x} \equiv \mathbf{0}$ into (21). We immediately get

$$v_y \equiv 0, \qquad B_z = 0, \tag{30}$$

and the new set of algebraic equations

$$\begin{cases} A_x + B_x &= m\omega_c^2 R, \\ A_y + B_y &= mg, \\ A_z &= mRc(\omega_c - \omega_0), \\ -A_z &= jmr\omega_c\tilde{\omega}_z, \\ A_x - B_y &= -jm\omega_c^2 R - jmr\omega_c\tilde{\omega}_x, \end{cases} \tag{31}$$

has to be solved for the different kinematic cases. In the next subsections, the resulting propositions can be proven by direct calculation; we present the details only for Case SS. Throughout this section, asymptotic stability, neutral stability and instability of solutions are considered within the corresponding phase spaces in the different kinematic cases. Stability with respect to slipping is discussed later in Sections 3-4.

2.1 Case RR

Proposition 1 *The stationary solution for* $\mathbf{f}_{\mathrm{RR}}$ *is*

$$\omega_c \equiv \omega_0, \tag{32}$$

which is asymptotically stable. For the stationary solution, $A_z = 0$ *and the contact force components* A_x*,* A_y*,* B_x*,* B_y *are undetermined.*

Due to the indeterminacy of the contact forces, the condition (13) cannot be checked.

2.2 Case RS

Proposition 2 *The stationary solutions for* $\mathbf{f}_{\mathrm{RS}}$ *are*

$$\begin{bmatrix} \omega_c \\ \tilde{\omega}_y \end{bmatrix} \equiv \begin{bmatrix} \omega_0 \\ \tilde{\omega}_y^0 \end{bmatrix}, \qquad \omega_0 = 0, \qquad \tilde{\omega}_y^0 \in \mathbb{R}, \tag{33}$$

which are neutrally stable with a zero eigenvalue. For the stationary solutions, the contact force components are

$$A_y = mg, \qquad A_x, A_z, B_x, B_y = 0. \tag{34}$$

This family of stationary solutions exists only for the single parameter value $\omega_0 = 0$ corresponding to zero velocity of the fluid flow. The ball is staying in one position, and it is spinning on the bottom of the vessel with a constant angular velocity $\tilde{\omega}_y^0$.

2.3 Case SR

Proposition 3 *The stationary solution for* $\mathbf{f}_{\mathrm{SR}}$ *is*

$$\begin{bmatrix} \omega_c \\ \tilde{\omega}_x \end{bmatrix} \equiv \begin{bmatrix} \omega_0 \\ \frac{g}{j\omega_0 r} - \omega_0 \frac{R}{r} \end{bmatrix}, \qquad \omega_0 \le \sqrt{\frac{g}{\eta R}}, \tag{35}$$

which is asymptotically stable for $\omega_0 > \sqrt{g/(jR)}$ *and unstable for* $\omega_0 < \sqrt{g/(jR)}$*. For the stationary solution, the contact force components are*

$$B_x = m\omega_0^2 R, \qquad B_y = mg, \qquad A_x, A_y, A_z = 0. \tag{36}$$

2.4 Case SS

Proposition 4 *The stationary solution for* $\mathbf{f}_{\mathrm{SS}}$ *is*

$$\begin{bmatrix} \omega_c \\ \tilde{\omega}_x \\ \tilde{\omega}_y \\ \tilde{\omega}_z \end{bmatrix} \equiv \begin{bmatrix} \omega_c^0(\alpha) \\ v_A^0(\alpha)/r \cdot \sin\alpha \\ 0 \\ v_A^0(\alpha)/r \cdot \cos\alpha \end{bmatrix}, \tag{37}$$

where

$$\omega_c^0(\alpha) = \sqrt{\tfrac{\mu g}{R}} \sqrt{\tfrac{1+\eta\cos^2\alpha}{(1+j\cos^2\alpha)\mu\eta+(j-\eta)\cos\alpha}}, \tag{38}$$

$$v_A^0(\alpha) = \tfrac{\mu g}{j\omega_c^0(\alpha)} \cdot \tfrac{-(j-\eta)\sin\alpha}{(1+j\cos^2\alpha)\mu\eta+(j-\eta)\cos\alpha}. \tag{39}$$

The solution (37) *exists for*

$$-\frac{\pi}{2} \le \alpha < 0, \qquad \eta \le j, \tag{40}$$

the parameter ω_0 *can be expressed as*

$$\omega_0(\alpha) = \omega_c^0(\alpha) - \tfrac{\frac{g\mu}{Rc}\cos\alpha\sin\alpha(j-\eta)}{(1+j\cos^2\alpha)\mu\eta+(j-\eta)\cos\alpha}, \tag{41}$$

and the normal force components are

$$\begin{aligned} A_y(\alpha) &= \tfrac{mg(j-\eta)\cos\alpha}{(1+j\cos^2\alpha)\mu\eta+(j-\eta)\cos\alpha}, \\ B_x(\alpha) &= \tfrac{\mu mg(1+j\cos^2\alpha)}{(1+j\cos^2\alpha)\mu\eta+(j-\eta)\cos\alpha}. \end{aligned} \tag{42}$$

Proof By using the slipping angle α defined in (8), the Coulomb law (16) becomes

$$A_x = -\mu A_y \cos\alpha, \qquad A_z = \mu A_y \sin\alpha. \tag{43}$$

By considering $B_z = 0$ from (30), the Coulumb law (17) results in

$$\tilde{\omega}_y \equiv 0, \qquad B_y = \eta B_x \operatorname{sgn} \tilde{\omega}_z = \eta B_x \operatorname{sgn} \cos\alpha. \tag{44}$$

If we substitute (8), (43) and (44) into (31), we get the system of equations

$$\begin{cases} -\mu A_y \cos\alpha + B_x - m\omega_c^2 R & = 0, \\ A_y + \eta B_x \operatorname{sgn} \cos\alpha & = mg, \\ \mu A_y \sin\alpha - mRc(\omega_c - \omega_0) & = 0, \\ -\mu A_y \sin\alpha - jm\omega_c v_A \cos\alpha & = 0, \\ -\mu A_y \cos\alpha - \eta B_x \operatorname{sgn} \cos\alpha & \\ \quad + jm\omega_c^2 R + jm\omega_c v_A \sin\alpha & = 0. \end{cases} \tag{45}$$

In the case $\cos\alpha < 0$, there is no solution, and in the case $\cos\alpha > 0$, we obtain (38), (39), (41) and (42). The conditions (40) are because of (12) and due to $v_A > 0$ in the case of slipping. □

Stability conditions for (37) cannot be expressed explicitly, they are computed numerically in Section 5. Equation (41) shows that $\omega_c^0 \neq \omega_0$, that is, even in the stationary case, there is a relative velocity between the ball and the surrounding fluid flow.

2.5 Case NR

Proposition 5 *The stationary solutions for* $\mathbf{f}_{\mathrm{NR}}$ *are*

$$\begin{bmatrix} y \\ v_y \\ \omega_c \\ \tilde{\omega}_x \end{bmatrix} \equiv \begin{bmatrix} y^0 \\ 0 \\ \omega_0 \\ \frac{g}{j\omega_0 r} - \omega_0 \frac{R}{r} \end{bmatrix}, \qquad \omega_0 \geq \sqrt{\frac{g}{\eta R}}, \tag{46}$$

which are neutrally stable with a zero eigenvalue. For the stationary solutions, the contact force components are

$$B_x = m\omega_0^2 R, \qquad B_y = mg, \qquad A_x, A_y, A_z = 0. \tag{47}$$

The stationary solutions (46) differ from each other only in the height y_0 where the ball is rolling around (see [6], p. 215 for a similar problem).

2.6 Case NS

It can be proved that (28) does not have a stationary solution. However, the coordinate y does not appear at the right side of (28), therefore, this *cyclic coordinate* can be separated from the system. That is, we get a reduced vector field $\hat{\mathbf{f}}_{\mathrm{NS}}$ with

$$\mathbf{f}_{\mathrm{NS}}(\mathbf{x}) = \begin{bmatrix} v_y \\ \hat{\mathbf{f}}_{\mathrm{NS}}(\hat{\mathbf{x}}) \end{bmatrix}, \tag{48}$$

where $\hat{\mathbf{x}} := \begin{bmatrix} v_y & \omega_c & \tilde{\omega}_x & \tilde{\omega}_y & \tilde{\omega}_z \end{bmatrix}^T \in \hat{X}$ is an element of the reduced phase space $\hat{X}$.

Proposition 6 *The stationary solution for* $\hat{\mathbf{f}}_{\mathrm{NS}}$ *is*

$$\begin{bmatrix} v_y \\ \omega_c \\ \tilde{\omega}_x \\ \tilde{\omega}_y \\ \tilde{\omega}_z \end{bmatrix} \equiv \begin{bmatrix} -\frac{g-\eta\omega_0^2 R}{c} \\ \omega_0 \\ \frac{\eta - j}{j}\omega_0 \frac{R}{r} \\ 0 \\ \frac{g-\eta\omega_0^2 R}{cr} \end{bmatrix}, \qquad \omega_0 < \sqrt{\frac{g}{\eta R}}, \tag{49}$$

which is neutrally stable with a pure imaginary pair $\pm i\omega_0$ *of eigenvalues. For the stationary solution, the contact force components are*

$$\begin{aligned} &B_x = m\omega_0^2 R, \qquad B_y = \eta m \omega_0^2 R, \\ &A_x, A_y, A_z = 0. \end{aligned} \tag{50}$$

Physically, (49) describes a motion where the axial (vertical) displacement of the ball decreases with a uniform speed v_y. Although (49) is a non-stationary solution of the original system $\mathbf{f}_{\mathrm{NS}}$, it interacts with (46) through a bifurcation. Note that (46) is a stationary solution both for $\mathbf{f}_{\mathrm{NS}}$ and $\hat{\mathbf{f}}_{\mathrm{NS}}$.

3 Stability with respect to slipping

In the previous section, the existence of the rolling were checked by using the condition (13). That is, the rolling motion at a contact point cannot exist if the magnitude of the tangential force is above a certain value. However, the condition of existence of rolling can be investigated from a different point of view. Physically, the rolling motion does not exist if a small perturbation can switch the system into permanent slipping. In this section, we introduce the mathematical description of this concept which can be called *stability with respect to slipping*.

3.1 Concept of stability with respect to slipping

Let us consider a mechanical system with rolling, which leads to a phase space Y and vector field $\mathbf{f}_Y$. Let us switch some of the rolling constraints into slipping with Coulomb friction, thus, we get a phase space Z and a vector field

$\mathbf{f}_Z$. The phase space Y of the rolling system is embedded into the phase space Z of the slipping system. For a point $\mathbf{x}^* \in Y$, let $W(\mathbf{x}^*)$ denote the orthogonal complement of Y at $\mathbf{x}^*$. That is, $W(\mathbf{x}^*)$ is the set of vectors that are orthogonal to Y at $\mathbf{x}^*$. The dimension

$$\dim W = \dim Z - \dim Y \tag{51}$$

is called the *codimension* of the subspace Y. We assume that $\mathbf{f}_Z$ is discontinuous in Y, hence, Y is called a *discontinuity surface* in Z.

Let Φ_Y and Φ_Z denote the flows of $\mathbf{f}_Y$ and $\mathbf{f}_Z$, respectively. Let us consider a trajectory $\Phi_Y(\mathbf{x}^*)$ of the rolling system. We would like to perturb this trajectory to switch the system into the slipping behaviour. For that, let us consider a vector $\mathbf{n} \in W(\mathbf{x}^*)$ normal to the space Y and let $\varepsilon \in \mathbb{R}^+$. Hence, the point $\mathbf{x}^* + \varepsilon\mathbf{n}$ is the *perturbed value of* $\mathbf{x}^*$ in the direction of $\mathbf{n}$. The perturbed value is outside Y, the slipping dynamics $\mathbf{f}_Z$ is valid there, and we get the *perturbed trajectory* $\Phi_Z(\mathbf{x}^* + \varepsilon\mathbf{n})$.

Let us define the quantity

$$\gamma(\mathbf{x}^*, \mathbf{n}) := \lim_{\varepsilon \to 0^+} \tfrac{\mathrm{d}}{\mathrm{d}t} \left(\Phi_Z(\mathbf{x}^* + \varepsilon\mathbf{n}) - \Phi_Y(\mathbf{x}^*)\right) \cdot \mathbf{n}, \tag{52}$$

which measures the rate of change of the distance between the perturbed and unperturbed trajectories in the direction of $\mathbf{n}$. As $\mathbf{n}$ is normal to $\mathbf{f}_Y$, (52) can be simplified to

$$\gamma(\mathbf{x}^*, \mathbf{n}) = \lim_{\varepsilon \to 0^+} \mathbf{f}_Z\left(\mathbf{x}^* + \varepsilon\mathbf{n}\right) \cdot \mathbf{n}. \tag{53}$$

If the value of (53) is nonzero, its sign determines if the slipping vector field points *towards* Y (in case of $\gamma < 0$) or points *away* from Y (in case of $\gamma > 0$) for the perturbed point $\mathbf{x}^* + \varepsilon\mathbf{n}$. If directions of all possible $\mathbf{n}$ are considered, we can introduce the following notions:

Definition 1 The point $\mathbf{x}^* \in Y$ is called *stable with respect to slipping* if $\gamma(\mathbf{x}^*, \mathbf{n}) < 0$ for all $\mathbf{n} \in W(\mathbf{x}^*)$.

Definition 2 The point $\mathbf{x}^* \in Y$ is called *unstable with respect to slipping* if there exists $\mathbf{n}_1 \in W(\mathbf{x}^*)$ for which $\gamma(\mathbf{x}^*, \mathbf{n}_1) > 0$.

Definition 3 The point $\mathbf{x}^* \in Y$ is called *neutrally stable with respect to slipping* if $\gamma(\mathbf{x}^*, \mathbf{n}) \leq 0$ for all $\mathbf{n} \in W(\mathbf{x}^*)$ and there exists $\mathbf{n}_1 \in W(\mathbf{x}^*)$ for which $\gamma(\mathbf{x}^*, \mathbf{n}_1) = 0$.

If a point is stable in this sense then we can create a temporary slipping by a small perturbation, but the slipping dynamics pulls the system back to the rolling behaviour. However, if a point is unstable in this sense then there exists a perturbation for which the dynamics pushes away the system from the rolling behaviour and permanent slipping begins.

Our definitions are in connection with Filippov's theory of piecewise smooth systems. If Y is a codimension-1 discontinuity surface in Z then it is also a *switching surface*. Then, the point $\mathbf{x}^*$ is stable in the sense of Definition 1 if and only if it is located in an *attracting sliding region* of Y (see [10] or [4], p. 76). However, there are higher codimension discontinuity surfaces in our system, where Filippov's theory is not applicable.

Note that some recent papers (see [16] and [8]) generalise Filippov's theory in the case of intersection of two sliding surfaces. This intersection leads to a special case of a codimension-2 discontinuity surface, but it still does not cover our problem. In our case, spatial slipping of rigid bodies at one contact point results in a codimension-2 discontinuity surface which cannot be composed from intersecting two codimension-1 discontinuity surfaces.

In the next subsection, the conditions of stability with respect to slipping are calculated in Case NR. Then, in Section 4, we apply the method for the stationary solution of Case RR.

3.2 Example: Transition from Case NR to Case NS

Let us consider the stability of Case NR with respect to slipping at point B. Then, with the notations of the previous subsection, $Y = X_{\mathrm{NR}}$, $Z = X_{\mathrm{NS}}$, $\mathbf{f}_Y = \mathbf{f}_{\mathrm{NR}}$ and $\mathbf{f}_Z = \mathbf{f}_{\mathrm{NS}}$. The dimensions are $\dim Y = 4$, $\dim Z = 6$, $\dim W = 2$, and Y is a codimension-2 discontinuity surface in Z.

At every point $\mathbf{x}^* \in X_{\mathrm{NR}}$, the orthogonal space W is the plane spanned by the coordinates $\tilde{\omega}_y$ and $\tilde{\omega}_z$. It is enough to consider the *unit vectors* from W, which can be parametrised easily by the slipping direction β,

$$\mathbf{n}(\beta) = \begin{bmatrix} 0 & 0 & 0 & 0 & \sin\beta & \cos\beta \end{bmatrix}^T, \qquad \beta \in [0, 2\pi). \tag{54}$$

That is, (53) can be also parametrised by β in the form

$$\gamma(\mathbf{x}^*, \beta) = \lim_{\varepsilon \to 0^+} \mathbf{f}_{\mathrm{NS}}(\mathbf{x}^* + \varepsilon\mathbf{n}(\beta)) \cdot \mathbf{n}(\beta). \tag{55}$$

Let us substitute the vector field $\mathbf{f}_{\mathrm{NS}}$ from (28) and compute the limit, then, we get

$$\gamma(\mathbf{x}^*, \beta) = \left(\tfrac{g}{r} + \tfrac{cv_y^*}{r} + \omega_c^*\tilde{\omega}_x^* + \tfrac{R}{r}(\omega_c^*)^2\right)\cos\beta + \\ + \tfrac{cR}{r}\left(\omega_0 - \omega_c^*\right)\sin\beta - \tfrac{\eta R(j+1)}{rj}(\omega_c^*)^2, \tag{56}$$

where $\mathbf{x}^* = \begin{bmatrix} y^*, v_y^*, \omega_c^*, \tilde{\omega}_x^*, 0, 0 \end{bmatrix}^T \in X_{\mathrm{NR}}$. According to Definition 1, the point $\mathbf{x}^*$ is stable with respect to slipping if (56) is negative for all β. As (56) is differentiable with respect to β, we can find the extreme values of $\gamma(\mathbf{x}^*, \beta)$ by solving

$$\frac{\mathrm{d}}{\mathrm{d}\beta}\gamma(\mathbf{x}^*, \beta) = 0, \tag{57}$$

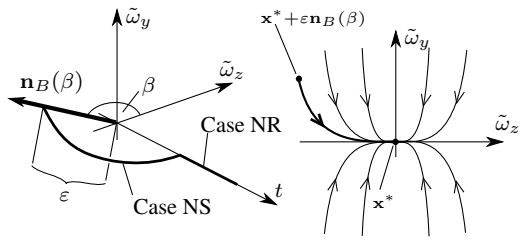

Fig. 4 Demonstration of a *stable* point with respect to slipping, the trajectory returns to Case NR. Left panel: Effect of perturbation in time. Right panel: Projection of the trajectories onto the orthogonal space.

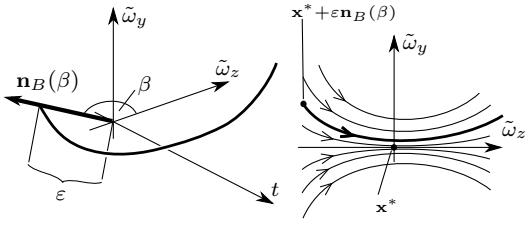

Fig. 5 Demonstration of a *unstable* point with respect to slipping, the trajectory remains in Case NS permanently. Left panel: Effect of perturbation in time. Right panel: Projection of the trajectories onto the orthogonal space.

from which we obtain the values

$$\beta_1 = \arctan \frac{\frac{cR}{r}\left(\omega_0 - \omega_c^*\right)}{\left(\frac{g}{r} + \frac{cv_y^*}{r} + \omega_c^*\tilde{\omega}_x^* + \frac{R}{r}(\omega_c^*)^2\right)}, \qquad (58)$$
$$\beta_2 = \beta_1 + \pi.$$

That is, $\mathbf{x}^*$ is stable with respect to slipping if

$$\gamma(\mathbf{x}^*, \beta_1) < 0 \qquad \text{and} \qquad \gamma(\mathbf{x}^*, \beta_2) < 0. \qquad (59)$$

By substituting (58) into (56), analytical formulae are obtained which determine a subset of stable points in X_{NR}.

For the stationary solution (46) of Case NR, $\beta_1 = 0$, $\beta_2 = \pi$ and we obtain

$$\begin{aligned}\gamma(\mathbf{x}^*, \beta_1) &= -\tfrac{j+1}{rj}\left(\eta R\omega_0^2 - g\right) < 0,\\ \gamma(\mathbf{x}^*, \beta_2) &= -\tfrac{j+1}{rj}\left(\eta R\omega_0^2 + g\right) < 0,\end{aligned} \qquad (60)$$

that is, (46) is stable with respect to slipping if

$$\omega_0 > \sqrt{\frac{g}{\eta R}}. \qquad (61)$$

In this case, the dynamics extinguishes the effect of the perturbation, and after a while, the ball returns to the stationary solution of Case NR (see Fig. 4). However, if $\omega_0 < \sqrt{g/(\eta R)}$ then the stationary solution is unstable with respect to slipping and the dynamics repels the trajectories away from the stationary solution of Case NR (see Fig. 5).

If only neutral stability is required then instead of (61), we get the same result as in (46), which was obtained from the requirement (13). By direct calculation from (27) and (56), one can check that this agreement is valid not only for the stationary solution but also for any point in X_{NR}. The reasons behind this coincidence can be explained from the properties of the simple Coulomb friction model (see [12], p. 85 and p. 139).

4 Stability with respect to slipping of the two-point rolling stationary motion

In this section, we focus on the stationary solution (32) of Case RR. As we mentioned in Subsection 2.1, condition (13) cannot be checked in this case. However, we can use the concept of stability with respect to slipping to determine the existence of (32).

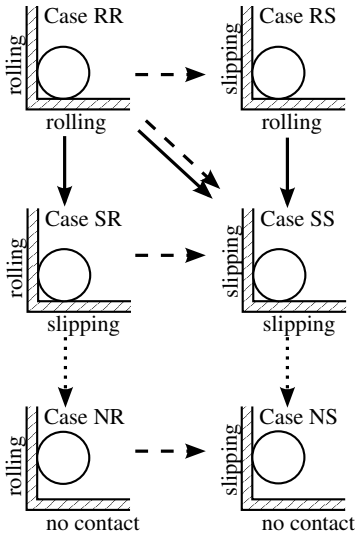

Fig. 6 Transitions to higher-order kinematic cases. Continuous arrows denote slipping at point A. Dashed arrows denote slipping at point B. Dotted arrows denote separation of the surfaces at point A.

With the notations of the previous section, let $Y = X_{\mathrm{RR}}$, $\mathbf{f}_Y = \mathbf{f}_{\mathrm{RR}}$, and let

$$\mathbf{x}^* = \left[\omega_c^*,\, 0,\, 0,\, 0,\, 0,\, 0\right]^T, \qquad \mathbf{x}^* \in X_{\mathrm{RR}} \qquad (62)$$

be a point of the state space of Case RR. In the following subsections, the stability of $\mathbf{x}^*$ is investigated with respect to slipping. Slipping is possible at A, B or both A and B (see Fig. 6), hence, transitions to Cases RS, SR and SS are analysed separately.

4.1 Transition to Case RS

Let us investigate slipping at point B, then, $Z = X_{\mathrm{RS}}$ and $\mathbf{f}_Z = \mathbf{f}_{\mathrm{RS}}$. In this codimension-1 case, the two possible unit

vectors of the one-dimensional orthogonal space W are denoted by

$$\mathbf{n}^{\pm} := \left[0\ 0\ 0\ 0\ \pm 1\ 0\right]^T. \tag{63}$$

With these, (53) can be written as

$$\gamma^{\pm}(\mathbf{x}^*) := \lim_{\varepsilon\to 0^+} \mathbf{f}_{\mathrm{RS}}(\mathbf{x}^* + \varepsilon\mathbf{n}^{\pm})\cdot\mathbf{n}^{\pm}. \tag{64}$$

In the case of stability with respect to slipping, we require

$$\gamma^{+}(\mathbf{x}^*) < 0 \qquad \text{and} \qquad \gamma^{-}(\mathbf{x}^*) < 0, \tag{65}$$

which result in

$$|\omega_c^* - \omega_0| - \frac{\mu}{jc}(1+j)(1+2j)(\omega_c^*)^2 < 0. \tag{66}$$

In the case of the stationary solution $\omega_c = \omega_0$, we get

$$\omega_0^2 > 0 \tag{67}$$

for the stability condition with respect to slipping at point B. This is violated only in the case $\omega_0 = 0$ when the system is neutrally stable. This corresponds to a bifurcation point; the stationary solutions (32) and (33) coincide if $\omega_0 = \tilde{\omega}_y = 0$.

As X_{RR} is a codimension-1 discontinuity surface of X_{RS}, it can be considered also as a switching surface and the results can be obtained also from Filippov's theorem. Let

$$\mathbf{f}_{\mathrm{RS}}^{\pm}(\mathbf{x}^*) := \lim_{\varepsilon\to 0^+} \mathbf{f}_{\mathrm{RS}}(\mathbf{x}^* + \varepsilon\mathbf{n}^{\pm}) \tag{68}$$

be the dynamics at the two sides of the switching surface. Then, the dynamics of Case RR is exactly the *sliding motion* of the system, which can be expressed from $\mathbf{f}_{\mathrm{RS}}^{+}$ and $\mathbf{f}_{\mathrm{RS}}^{-}$ by using Filippov's convex method (see [4], p. 76). That is, there exists $\delta(\mathbf{x}^*) : X_{\mathrm{RR}} \to \mathbb{R}$ for that

$$\mathbf{f}_{\mathrm{RR}} = \delta\cdot\mathbf{f}_{\mathrm{RS}}^{-} + (1-\delta)\cdot\mathbf{f}_{\mathrm{RS}}^{+}. \tag{69}$$

It can be checked that the condition $0 < \delta < 1$ of the attracting sliding region is equivalent to the stability condition (64) with respect to slipping.

4.2 Transition to Case SR

Let us now investigate slipping at point A, thus, $Z = X_{\mathrm{SR}}$, $\mathbf{f}_Z = \mathbf{f}_{\mathrm{SR}}$, and the unit vectors of W are denoted by

$$\mathbf{n}^{\pm} := \left[0\ 0\ 0\ \pm 1\ 0\ 0\right]^T. \tag{70}$$

In this case, (53) becomes

$$\gamma^{\pm}(\mathbf{x}^*) := \lim_{\varepsilon\to 0^+} \mathbf{f}_{\mathrm{SR}}(\mathbf{x}^* + \varepsilon\mathbf{n}^{\pm})\cdot\mathbf{n}^{\pm}. \tag{71}$$

The point $\mathbf{x}^*$ is stable with respect to slipping if

$$\gamma^{+}(\mathbf{x}^*) < 0 \qquad \text{and} \qquad \gamma^{-}(\mathbf{x}^*) < 0, \tag{72}$$

which leads to

$$|\omega_c^* - \omega_0| - \frac{(1+2j)\mu}{jRc}\left(g - jR(\omega_c^*)^2\right) < 0. \tag{73}$$

In the stationary case $\omega_c = \omega_0$, we get

$$\omega_0 < \sqrt{\frac{g}{jR}} \tag{74}$$

for the stability condition with respect to slipping. At the neutrally stable case $\omega_0 = \sqrt{g/(jR)}$, the stationary solutions (32) and (35) coincide.

As in the previous subsection, transition to Case SR could be investigated also by Filippov's theorem because X_{RR} is a codimension-1 discontinuity surface of X_{SR}.

4.3 Transition to Case SS

In this case, we investigate slipping at *both* points A and B. This situation cannot be composed from the two previous cases because the rolling conditions at A and B are not independent.

With the previous notations, $Z = X_{\mathrm{SS}}$, $\mathbf{f}_Z = \mathbf{f}_{\mathrm{SS}}$, and X_{RR} is a codimension-3 discontinuity set of X_{SS}. That is, the orthogonal space W is 3 dimensional and the unit vectors of W are located on a two dimensional unit sphere. By using the slipping directions α and β, this sphere can be parametrised as

$$\mathbf{n}(\alpha,\beta) := \frac{\operatorname{sgn}(\pi/2-\alpha)}{\sqrt{1+\tan^2\alpha+\tan^2\beta}}\cdot\left[0,\,0,\,0,\,\tan\alpha,\,\tan\beta,\,1\right]^T, \tag{75}$$

where

$$(\alpha,\beta)\in\mathcal{A} := [-\tfrac{\pi}{2},\tfrac{\pi}{2}]^2 \cup [\tfrac{\pi}{2},\tfrac{3\pi}{2}]^2. \tag{76}$$

This parametrisation is singular at $\alpha,\beta = \pm\pi/2$. With these parameters, (53) can be formulated as

$$\gamma(\mathbf{x}^*,\alpha,\beta) := \lim_{\varepsilon\to 0^+} \mathbf{f}_{\mathrm{SS}}(\mathbf{x}^* + \varepsilon\mathbf{n}(\alpha,\beta))\cdot\mathbf{n}(\alpha,\beta). \tag{77}$$

If $\mathbf{x}^*$ is stable with respect to slipping then (77) is negative for any $(\alpha,\beta)\in\mathcal{A}$. The local extrema can be found by

$$\frac{\mathrm{d}}{\mathrm{d}\alpha}\gamma(\mathbf{x}^*,\alpha,\beta) = 0, \qquad \frac{\mathrm{d}}{\mathrm{d}\beta}\gamma(\mathbf{x}^*,\alpha,\beta) = 0. \tag{78}$$

If we substitute the vector field (26) and the stationary solution $\omega_c = \omega_0$ into (78), we get a system of equations in α and β in the form

$$\mathbf{C}(\cos\alpha^*,\cos\beta^*)\cdot\begin{bmatrix}\sin\alpha^*\\ \sin\beta^*\end{bmatrix} = \begin{bmatrix}0\\0\end{bmatrix}, \tag{79}$$

where $\mathbf{C}$ is a two-by-two matrix including lengthy algebraic expressions in its elements. The trivial solution is $\sin\alpha = \sin\beta = 0$, and according to (76), the possible pairs are

$$(\alpha_1, \beta_1) = (0, 0), \qquad (\alpha_2, \beta_2) = (\pi, \pi). \tag{80}$$

It can be checked numerically that the values (80) correspond to the global extrema of $\gamma(\mathbf{x}^*, \alpha, \beta)$ in $\mathcal{A}$. Thus, we require

$$\gamma(\mathbf{x}^*, 0, 0) < 0 \qquad \text{and} \qquad \gamma(\mathbf{x}^*, \pi, \pi) < 0 \tag{81}$$

in the case when $\mathbf{x}^*$ is stable with respect to slipping. From these conditions, we get

$$\omega_0 < \sqrt{\tfrac{g}{\eta R}} \cdot \sqrt{\tfrac{\mu\eta(\eta+1)}{\mu\eta(1+j)+j-\eta}}, \tag{82}$$

$$\omega_0 > \sqrt{\tfrac{g}{\eta R}} \cdot \sqrt{\tfrac{\mu\eta(\eta-1)}{\mu\eta(1+j)+j+\eta}}, \tag{83}$$

respectively.

From calculating the normal force components A_y and B_x by using (29) and (80), we get that the stability loss at the critical value of (83) contradicts to (12). From similar reasons, we get that the stability loss at the critical value of (82) can occur only if $\eta < j$.

5 Bifurcations of the system

During the following analysis, we choose ω_0 as the primary bifurcation parameter, and we focus also on the friction coefficients η and μ because they have the most significant effect on the qualitative behaviour of the system.

Besides usual bifurcations of smooth systems, we have to deal with bifurcations caused by the discontinuities of the system. These bifurcations are generally called *discontinuity-induced bifurcations* (DIBs), and the term *boundary equilibrium bifurcation* (BEB) is used for the cases when equilibrium points interact with discontinuity surfaces. These types of bifurcations are explained e.g. in [5], [19] and [20], or see the textbooks [4] and [21] for a deeper overview of the topic. Besides the discontinuity-induced variants of the basic bifurcation types (e.g. nonsmooth fold), BEBs include the *persistence* (or *border-crossing*) bifurcation, when an equilibrium passes through a discontinuity surface.

5.1 Bifurcation surfaces in the parameter space

From the previous sections, let us collect the values of ω_0 for which the number of the stationary solutions change in the different kinematic cases. From (40) and (41), let us define

$$\omega_{01} := \omega_0(0) = \sqrt{\tfrac{g}{\eta R}}\sqrt{\tfrac{\mu\eta(\eta+1)}{\mu\eta(1+j)+j-\eta}}, \tag{84}$$

which value appears also in (82). Similarly, let us define

$$\omega_{02} := \omega_0\left(-\frac{\pi}{2}\right) = \sqrt{\tfrac{g}{\eta R}}, \tag{85}$$

which we obtained also in (35), (46) and (49). Finally, let us define

$$\omega_{03} := \sqrt{\frac{g}{jR}}, \tag{86}$$

which appears in (74). We can see later that the values $\omega_{01} - \omega_{03}$ correspond to discontinuity-induced bifurcations of the system. However, we can also find a usual fold bifurcation in Case SS:

Proposition 7 *Let us consider* $\omega_0(\alpha)$ *from* (41) *and let*

$$j > \eta > \eta_{cr} := \frac{c^2 R}{4g\mu^2}. \tag{87}$$

Then, there exists $\hat{\alpha} \in [-\pi/2, 0]$ *for that there is a fold bifurcation of the stationary solution* (37) *at*

$$\omega_{04} := \omega_0(\hat{\alpha}). \tag{88}$$

Proof Let

$$w(\alpha) := \frac{\mathrm{d}\omega_0}{\mathrm{d}\alpha}(\alpha). \tag{89}$$

It can be checked by direct calculation that if (87) is satisfied then $w(-\pi/2) > 0$ and $w(0) < 0$. As $w(\alpha)$ is continuous, Bolzano's theorem guarantees the existence of $\hat{\alpha} \in [-\pi/2, 0]$ for that $w(\hat{\alpha}) = 0$. By using the chain rule,

$$\frac{\mathrm{d}\omega_0}{\mathrm{d}\omega_c}(\hat{\alpha}) = \frac{w(\hat{\alpha})}{\frac{\mathrm{d}\omega_c}{\mathrm{d}\alpha}(\hat{\alpha})}, \qquad \frac{\mathrm{d}\omega_0}{\mathrm{d}v_A}(\hat{\alpha}) = \frac{w(\hat{\alpha})}{\frac{\mathrm{d}v_A}{\mathrm{d}\alpha}(\hat{\alpha})} \tag{90}$$

are both zero. This results in a fold bifurcation of the stationary solution (37) at $\omega_0 = \omega_{04}$. □

We can check numerically that there exists only one such ω_{04}, and $\omega_{04} > \max(\omega_{01}, \omega_{02})$. The stable branch of the solution exists for $\omega_0 \in [\omega_{01}, \omega_{04}]$ the unstable branch exists for $\omega_0 \in [\omega_{02}, \omega_{04}]$.

The surfaces ω_{01}–ω_{04} divide the parameter space into regions where the number of the equilibria remains the same for each kinematic case. This can be seen in Figs. 7 and 8. Inside the different regions, the kinematic cases are denoted where corresponding equilibria exist. In Case RS, equilibria exist only on the axis $\omega_0 = 0$, this case is not denoted in the graphs.

In Fig. 7, the value of μ is fixed, and the value of η is varied along the horizontal axis. In Fig. 8, values of $\mu = \eta$ are varied together. The two cases result in similar graphs. The main difference is, that, for fixed value of μ (Fig. 7), there exists an equilibrium in Case RR also for $\eta = 0$, up to a certain value of ω_0.

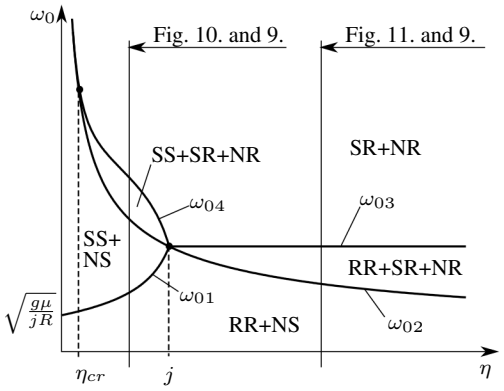

Fig. 7 Bifurcation surfaces in the parameter space, all parameters are fixed except ω_0 and η.

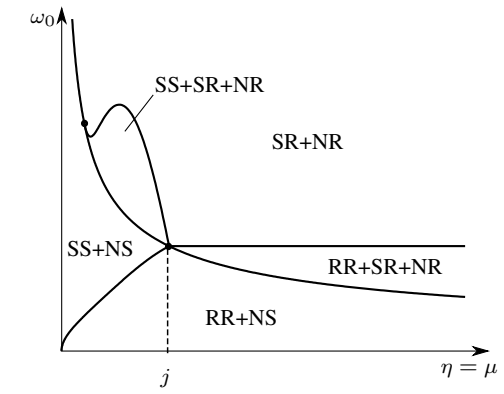

Fig. 8 Bifurcation surfaces in the parameter space, all parameters are fixed except ω_0 and $\eta = \mu$.

On the boundaries, some equilibria appear or vanish, which correspond to codimension-1 bifurcations explained below. The intersections of these boundaries (denoted by black dots in Figs. 7 and 8) correspond to higher codimension bifurcations, which are not analysed in this paper. In Fig. 7, the values of η for these higher codimension bifurcations are $\eta = j$ and $\eta = \eta_{cr}$. It is denoted in Fig. 7, that typical values of η are chosen from the intervals (η_{cr}, j) and (j, ∞) for which we determine the bifurcation diagrams in the next subsection. Note that according to (10) and (87), the order of the magnitude of $\eta_{cr} \cdot \mu^2$ is below 10^{-6} for physically realistic parameters, thus, the case $\eta < \eta_{cr}$ is practically irrelevant.

Let us emphasise that the *codimension of the bifurcation* (in the parameter space) is different from the *codimension of the discontinuity set* (in the phase space). For example, all the bifurcations in Table 5 are codimension-1, and the codimension of the corresponding discontinuity sets are denoted in brackets.

Value	Bifurcation	Notation	Cases
ω_{01}	persistence (codimension-3)	P3	RR–SS
ω_{02}	nonsmooth fold (codimension-2)	NF2	SS–SR
ω_{02}	persistence (codimension-2)	P2	NS–NR
ω_{03}	nonsmooth transcritical (codimension-1)	NT1	RR–SR
ω_{04}	fold	F	SS

Table 5 Bifurcation values of ω_0 with the name and abbreviation of the bifurcation and the corresponding kinematic cases.

5.2 Bifurcation diagrams

In the different kinematic cases, the equilibrium solutions are located in different subspaces of X. Thus, for the full bifurcation diagram of ω_0, a 7-dimensional graph would be needed. If we want to describe the location of the equilibria by a single variable, the natural choice of ω_c does not result in clear bifurcation diagrams due to overlapping of curves (see Fig. 13). Instead, let us define

$$\omega_x^0 := \tilde{\omega}_x^0 + \frac{R}{r}\omega_c^0, \tag{91}$$

where $\omega_c \equiv \omega_c^0$ and $\tilde{\omega}_x \equiv \tilde{\omega}_x^0$ are the coordinates of the stationary solution. Physically, (91) means the angular velocity of spinning on the wall (the first coordinate of (4)).

Equilibria of the system can be visualised more clearly if they are divided into two groups. In Cases NS and NR, the ball is on the wall being separated from the ground. In Cases RR, SR and SS, the ball is on the bottom of the vessel. All occurring bifurcations are summarised in Table 5 and we explain them in details in the next paragraphs.

Bifurcation diagram for Cases NS and NR can be seen in Fig. 9. Bifurcation of these cases appears on the surface ω_{02} and qualitatively the same diagram is obtained for both sections of Fig. 7. At $\omega_0 = \omega_{02}$, the stationary solution of Case NS vanishes as it reaches X_{NR}, which is a codimension-2 discontinuity set of X_{NS}. Simultaneously, an equilibrium point of Case NR appears. From another point of view, the equilibrium point gets stuck into the lower dimensional discontinuity set. This bifurcation can be called a *persistence* bifurcation, if the notion (see e.g. [4], p. 221) is generalised for discontinuity sets with a higher codimension. On the diagrams, this bifurcation is denoted by P2.

In the cases where $y \equiv 0$, we get rather different bifurcation diagrams for the two sections of Fig. 7. For $\eta < j$, the diagram in Fig. 10 is obtained. At $\omega_0 = \omega_{01}$, the equilibrium point of Case RR disappears, and an equilibrium point of Case SS appears. We can also say that the equilibrium point leaves X_{RR} which is a codimension-3 discontinuity set of X_{SS}. As in the previous case, this can be also called

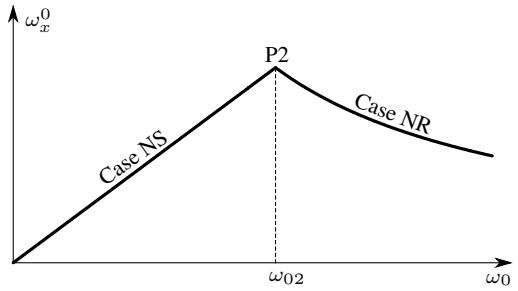

Fig. 9 Bifurcation diagram for $y > 0$, which is valid both for $\eta < j$ and $\eta > j$. This diagram contains only the equilibria, where the ball is separated from the ground (Cases NR and NS), and y is a cyclic coordinate.

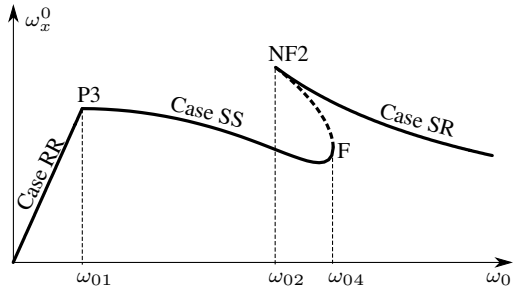

Fig. 10 Bifurcation diagram for $\eta < j$ and $y \equiv 0$. The dashed line denotes an unstable equilibrium within $X_{\rm SS}$.

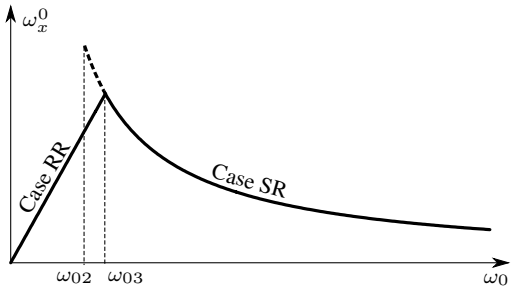

Fig. 11 Bifurcation diagram for $\eta > j$ and $y \equiv 0$. The dashed line denotes an unstable equilibrium within $X_{\rm SR}$. At ω_{02} and ω_{03}, bifurcations appear, but their type cannot be determined due to the degeneracy of the system.

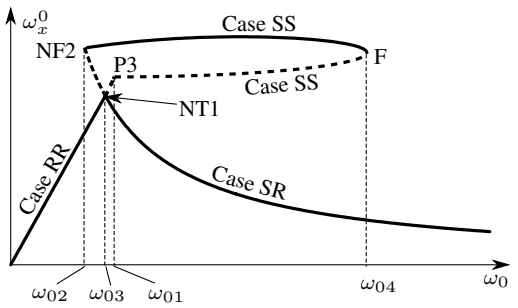

Fig. 12 Bifurcation diagram for $\eta > j$ and $y \equiv 0$, where (12) is released, that is, $A_y < 0$ is allowed. Dashed lines denote unstable equilibria.

a persistence bifurcation, which is denoted by P3 in the diagrams. At $\omega_0 = \omega_{04}$, a fold occurs between the stable and unstable equilibria of Case SS (denoted by F). At $\omega_0 = \omega_{02}$, the stable equilibrium of Case SR and the unstable equilibrium of Case SS collapses. This can be called a *nonsmooth fold*, and we denote it by NF2, as $X_{\rm SR}$ is a codimension-2 subset of $X_{\rm SS}$.

For $\eta > j$, we get the bifurcation diagram in Fig. 11. There are discontinuity-induced bifurcations at $\omega_0 = \omega_{02}$ and $\omega_0 = \omega_{03}$, but their type is unclear, because some equilibria seem to vanish. It is because of the degenerate equilibria of the system. Let us emphasise, that equilibria (35) and equilibrium (46) coincide if $y^0 = 0$, that is, equilibrium of Case SR is connected to a (degenerate) family of equilibria of Case NR (compare Figs. 9 and 11).

This degeneracy of the system can be resolved if condition (12) is ignored, that is, we allow the traction $A_y < 0$. Then, we get the bifurcation diagram in Fig. 12. Of course, this diagram is not valid for our physical system, but this modification helps us to understand the bifurcations of the real system. In Fig 12, all the bifurcations appear, which we found in the case $\eta < j$ (P3, F and NF2, see Fig. 10). Moreover, we get a further bifurcation at $\omega_0 = \omega_{03}$. By increasing ω_0 through ω_{03}, the unstable equilibrium of Case SR reaches $X_{\rm RR}$, where it meets the stable equilibrium of Case RR, and it becomes stable. In the interval $\omega_{03} < \omega_0 < \omega_{01}$, the equilibrium of Case RR is unstable with respect to slipping to Case SR from *all* directions (see (73)), which is called a *virtual pseudo-equilibrium* (see [4], p. 234). That is, the bifurcation at $\omega_0 = \omega_{03}$ can be called a *nonsmooth transcritical bifurcation* (see also [20]), which is denoted by NT1 on the graph.

By understanding the bifurcations in Fig. 12, we can summarize, that we can find the degenerate variants of the discontinuity-induced bifurcations NF2 and NT1 at ω_{02} and ω_{03}, respectively, in our physically correct bifurcation diagram (Fig. 11).

5.3 Limitations of operation of the flowmeter

As it was mentioned in the introduction, operation of the flowmeter is based on measuring the velocity of the ball around the vessel, which means measurement of $\omega_c(t)$. For stationary flow velocity characterised by ω_0, a constant $\omega_c(t) \equiv \omega_c^0$ value is measured if we are in the bases of attraction of the stationary solutions. In the descriptions of many patents, it is explicitly assumed that the ball remains in the case of dual-point rolling (Case RR) with $\omega_c^0(t) \equiv \omega_0$, but we have seen that the situation is much more complicated.

In Fig. 13, we can see theoretical characteristic curves of the flowmeter which are based on the results of the previous subsections. In the left panel of Fig. 13, it can be seen, that

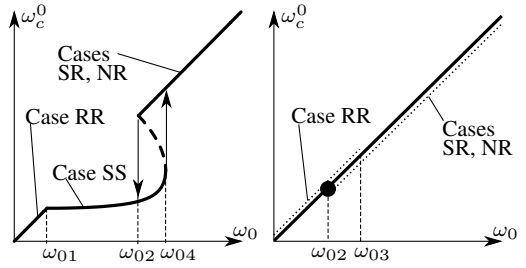

Fig. 13 Characteristic curves of the possible flowmeter. Left panel: for $\eta < j$, the arrows denote the hysteresis effect. Right panel: $\eta > j$, coincidence between curves of the different cases are made unambiguous by the dotted lines. The black dot denote the location of transient effects at unloading.

in the case $\eta < j$, the dual-point slipping causes complications. At $\omega_0 = \omega_{01}$, the stationary solution passes over to Case SS, and there is a jump in the slope of the characteristic curve. Between ω_{01} and ω_{02}, calibration of the flowmeter is possible, but for physically realistic parameters, the slope of the curve is very small here, which decreases the accuracy of the flowmeter. Between ω_{02} and ω_{04}, two co-existing stable stationary solutions can be found. This causes a hysteresis effect (denoted by arrows in Fig. 13) and makes the calibration impossible in this region. In the case $\omega_0 > \omega_{02}$, the co-existing stationary solutions of Cases SR and NR correspond to $\omega_c^0 = \omega_0$, which can be used for measurement, again.

On the right panel of Fig. 13, the case $\eta > j$ can be seen. The stationary solutions of Cases RR, SR and NR all overlap on the line $\omega_c^0 = \omega_0$, which results in a more favourable dynamics for the flowmeter. However, the motion corresponding to Case RR is different from the others (see also Fig. 11), because other coordinates of the solution do not coincide. If in the region $\omega_0 > \omega_{03}$, a small perturbation pushes the stationary solution from Case SR to Case NR, the dynamics can remain in this case also for slow decreasing of ω_0 between ω_{02} and ω_{03}. As the characteristic curves of Cases RR and NR coincide, this hysteresis effect is interesting only when we reach ω_{02} by decreasing ω_0 (see the black dot in Fig. 13). Then, the stationary solution of Case NR vanishes, and after a temporary existing solution of Case NS (see Fig. 9), transient effects and impacts can occur before reaching the stationary solution of Case RR. This is, again, unfavourable from the point of view of the measurement.

To summarize, we can say, that in both cases of Fig. 13, transitions between different kinematic cases and bifurcations cause limitations in favourable operation of the flowmeter. To keep the stationary solution in Case RR, one possible strategy is to increase the values of ω_{01} (if $\eta < j$) and ω_{02} (if $\eta > j$) through the parameters of the system. Alternatively, shape of the swirling blades could be tuned to reach not too large values of ω_0. Too much reduction in ω_0, however, results in inaccuracy in the measurement of the velocity of the ball.

Let us emphasise, that our analysis was restricted to the stationary solutions in the case of stationary fluid flow. Possible existence of periodic or chaotic attractors of the system and effects of transient flow may cause further problems in usage of these types of flowmeters.

6 Conclusion

We analysed a model of a concept of a type of a flowmeter which contains a ball moving round in a cylindrical vessel. Due to the slipping and unilateral contact at both contact points, nine kinematic cases of the system are possible. By assuming Coulomb's friction law for slipping and Stokes's drag law for the fluid, we derived the equations of motion for the different cases which build a nonsmooth dynamical system.

We determined the stationary solutions of the different cases and determined their stability within the current kinematic case. Limitations of existence of stationary solutions were investigated from restrictions of the contact forces, which could not be done in the dual-point rolling case when the forces are undetermined.

We introduced the concept of stability with respect to slipping, which can be used for determining the existence of solutions in the lower-dimensional kinematic cases without determining all contact forces. By this method, we determined conditions of existence of the stationary motion also in the dual-point rolling case.

Bifurcations of the system were investigated focusing on the parameters of the fluid velocity ω_0 and the friction coefficients μ and η. We discovered several nonsmooth bifurcations in the system such as persistence bifurcation, nonsmooth fold and nonsmooth transcritical bifurcation.

From the results, we were able to show qualitative limitations of the concept of this flowmeter that arise from the nonsmooth behaviour of the dual-point contact of the ball. If the fluid flow is modelled more accurately, then, based on our results, also quantitative results can be obtained for a given geometry of the flowmeter.

Acknowledgements The research leading to these results has received funding from the European Research Council under the European Union's Seventh Framework Programme (FP/2007-2013) / ERC Advanced Grant Agreement n. 340889. We thank Csaba Hos of the University of Technology and Economics for the useful comments. We thank the reviewers for the useful critical comments and suggestions.

Final publication: The final publication is available at Springer via http://dx.doi.org/10.1007/s11071-015-2356-y.

References

1. Antali, M., Stepan, G.: Nonlinear kinematic oscillations of railway wheelsets of general surface geometry. Proc. Appl. Math. Mech. **14**, 303–304 (2014)
2. Antali, M., Stepan, G., Hogan, J.: Kinematic oscillations of railway whellsets. Multibody System Dynamics **34**(3), 259–274 (2015)
3. Antoine, J.F., Abba, G., Molinari, A.: A new proposal for explicit angle calculation in angular contact ball bearing. Journal of Mechanical Design **128**, 468–478 (2005)
4. di Bernardo, M., Budd, C.J., Champneys, A.R., Kowalczyk, P.: Piecewise-smooth Dynamical Systems. Springer (2008)
5. di Bernardo, M., Hogan, S.J.: Discontinuity-induced bifurcations of piecewise smooth dynamical systems. Phil. Trans. R. Soc A. **368**, 4915–4935 (2010)
6. Bloch, A.M.: Nonholonomic mechanics and control. Springer (2003)
7. Campau, D.N.: Fluid flow indicator. US Patent, US 4 819 577 (1989)
8. Dieci, L., Difonzo, F.: The moments sliding vector field on the intersection of two manifolds. Journal of Dynamics and Differential Equations (2015, online first). DOI 10.1007/s10884-015-9439-9
9. Eldridge, G., Eldridge, R.: Cyclonic flow meters. US Patent, US 5 905 200 (1999)
10. Filippov, A.: Differential Equations with Discontinuous Right-hand Sides. Kluwer Acedemic Publishers (1988)
11. Gilbert, K.W.: Volumetric fluid flow meter. UK Patent, GB 1 246 779 (1970)
12. Glocker, C.: Set-Valued Force Laws. Springer (2001)
13. Greenwood, D.T.: Advanced Dynamics. Cambridge University Press (2003)
14. Hamrock, B.J.: Ball motion and sliding friction in an arched outer race ball bearing. Journal of Tribology **97**(2), 202–2010 (1975)
15. Houlberg, D.M.: Fluid flow meter. US Patent, US 4 089 220 (1978)
16. Jeffrey, M.R.: Dynamics at a switching intersection: Hierarchy, isonomy, and multiple sliding. SIAM J. Appl. Dyn. Syst. **13**(3), 1082–1105 (2014)
17. Kearsley, W.K.: Flowmeter. US Patent, US 2 518 149 (1950)
18. Kurose, R., Komuri, S.: Drag and lift forces on a rotating sphere in a linear shear flow. Journal of Fluid Mechanics **384**, 183–206 (1999)
19. Kuznetsov, Y.A., Rinaldi, S., Gragnani, A.: One-parameter bifurcations in planar Filippov systems. International Journal of Bifurcations and Chaos **13**(8), 2157–2188 (2003)
20. Leine, R.I., van Campen, D.H., van de Vrande, B.H.: Bifurcations in nonlinear discontinuous systems. Nonlinear Dynamics **23**(2), 105–164 (2000)
21. Leine, R.I., Nijmeijer, H.: Dynamics and Bifurcations in Non-Smooth Mechanical Systems. Springer (2004)
22. Lemaitre, J. (ed.): Handbook of Materials Behavior Models. Academic Press (2001)
23. Le Saux, C., Leine, R.I., Glocker, C.: Dynamics of a rolling disk in the presence of dry friction. Journal of Nonlinear Science **15**, 27–61 (2005)
24. Noel, D., Rithou, M., Furet, B., Noch, S.L.: Complete analytical expression of the stiffness matrix of angular contact ball bearings. Journal of Tribology **135**(4), DOI: 10.1115/1.4024,109 (2013)
25. de Pater, A.D.: The equations of motion of a dicone moving on a pair of circular cylinders. Int. J. Non-linear Mechanics **20**, 439–449 (1985)
26. Peters, M.L.J.P.: Orbital ball flow meter for liquids and gases. World Intellectual Property Organization, WO 01/25829 A1 (2001)
27. Peters, M.L.J.P.: Orbital ball flowmeter for gas and fluis. US Patent, US 8 505 378 B2 (2013)
28. Pritchard, P.J.: Introduction to Fluid Mechanics, 8 edn. Wiley (2011)
29. Rubinov, S.I., Keller, J.B.: The transverse force on a spinning sphere moving in a viscous fluid. Journal of Fluid Mechanics **11**(3), 447–459 (1961)
30. Sallai, G.: Dispositif de mesure pour ecoulements fluidiques. French Patent, FR 2 368 698 (1978)
31. Shaw, S.: On the dynamic response of a system with dry friction. Journal of Sound and Vibration **108**(2), 305–325 (1986)
32. Wickens, A.H.: The dynamic stability of railway vehicle wheelsets and bogies having profiled wheels. Int. J. Solids Structures **1**, 319–341 (1965)
33. Yukinori, O., Shui, Y.: Flow rate detecting device. European Patent Office, EPO 0 172 451 (1986)
34. Zhao, J.S., et al.: Effects of gyroscopic moment on the damage of a tapered roller bearing. Mechanism and Machine Theory **69**, 185–199 (2013)